Am J Nucl Med Mol Imaging 2015;5(2):127-142
www.ajnmmi.us /ISSN:2160-8407/ajnmmi0003365

Original Article

Combined use of ^{18}F-FDG and ^{18}F-FMISO in unresectable non-small cell lung cancer patients planned for radiotherapy: a dynamic PET/CT study

Christos Sachpekidis[1], Christian Thieke[2,3], Vasileios Askoxylakis[2,3], Nils H Nicolay[2,3], Peter E Huber[2,3], Michael Thomas[4], Georgia Dimitrakopoulou[1], Juergen Debus[2,3], Uwe Haberkorn[1,5], Antonia Dimitrakopoulou-Strauss[1]

[1]Clinical Cooperation Unit Nuclear Medicine, German Cancer Research Center, Heidelberg, Germany; [2]Clinical Cooperation Unit Radiotherapy, German Cancer Research Center, Heidelberg, Germany; [3]Department of Radiation Oncology, University Clinic Heidelberg, Germany; [4]Department Thoracic Oncology/Internal Medicine, Thoraxklinik, University of Heidelberg, Germany; [5]Division of Nuclear Medicine, University of Heidelberg, Germany

Received October 24, 2014; Accepted November 19, 2014; Epub January 15, 2015; Published February 1, 2015

Abstract: Aim of this study was to evaluate and compare, by means of dynamic and static PET/CT, the distribution patterns and pharmacokinetics of fluorine-18 fluorodeoxyglucose (^{18}F-FDG) and of fluorine-18-fluoromisonidazole (^{18}F-FMISO) in non-small cell lung cancer (NSCLC) patients scheduled for intensity modulated radiation therapy (IMRT). Thirteen patients suffering from inoperable stage III NSCLC underwent PET/CTs with ^{18}F-FDG and ^{18}F-FMISO for tumor metabolism and hypoxia assessment accordingly. Evaluation of PET/CT studies was based on visual analysis, semi-quantitative (SUV) calculations and absolute quantitative estimations, after application of a two-tissue compartment model and a non-compartmental approach. ^{18}F-FDG PET/CT revealed all thirteen primary lung tumors as sites of increased ^{18}F-FDG uptake. Six patients demonstrated also in total 43 ^{18}F-FDG avid metastases; these patients were excluded from radiotherapy. ^{18}F-MISO PET/CT demonstrated 12/13 primary lung tumors with faint tracer uptake. Only one tumor was clearly ^{18}F-FMISO avid, ($SUV_{average}$ = 3.4, SUV_{max} = 5.0). Mean values for ^{18}F-FDG, as derived from dPET/CT data, were $SUV_{average}$ = 8.9, SUV_{max} = 15.1, K_1 = 0.23, k_2 = 0.53, k_3 = 0.17, k_4 = 0.02, influx = 0.05 and fractal dimension (FD) = 1.25 for the primary tumors. The respective values for ^{18}F-FMISO were $SUV_{average}$ = 1.4, SUV_{max} = 2.2, K_1 = 0.26, k_2 = 0.56, k_3 = 0.06, k_4 = 0.06, influx = 0.02 and FD = 1.14. No statistically significant correlation was observed between the two tracers. ^{18}F-FDG PET/CT changed therapy management in six patients, by excluding them from planned IMRT. ^{18}F-FMISO PET/CT revealed absence of significant tracer uptake in the majority of the ^{18}F-FDG avid NSCLCs. Lack of correlation between the two tracers' kinetics indicates that they reflect different molecular mechanisms and implies the discordance between increased glycolysis and hypoxia in the malignancy.

Keywords: ^{18}F-FDG, ^{18}F-FMISO, PET/CT, non-small cell lung cancer, hypoxia

Introduction

Lung cancer is the most common cause of cancer mortality, with non-small cell lung cancer (NSCLC) accounting for almost 80% of all cases. In 2014 the estimated new cases of lung cancer in US are 224,210, while the estimated deaths attributed to the malignancy are 159,260 [1]. The treatment of choice is surgical resection of the tumor and the draining lymph nodes. This therapeutic approach applies to patients classified in stages I-IIIA of the disease [2]. However, a radical resection is possible in only 20% of all NSCLC cases [3]. In cases of advanced, unresectable NSCLC (IIIB and IV) radiotherapy, chemotherapy or their combinations represent the standard of care. Particularly in stage IIIB NSCLC, which is the population studied in the present paper, the application of chemotherapy combined with radiation therapy results in better results than radiation therapy alone [4-6]. However, the vast majority of patients presenting with stage IIIB NSCLC still demonstrate low survival rates with an anticipated 5-year survival ranging from 3% to 7% [7]. In these terms, the identification of factors that can affect treatment response is highly important; on one side, it could lead to the selection only of those candidates who would

benefit most from the applied treatment and, on the other side, it could contribute to the exclusion of those patients that are not expected to benefit from certain therapeutical approaches and, thus, avoid undergoing treatments, many of which carry some serious side-effects.

Tumor hypoxia has been recognized as an adverse prognostic factor for many cancer types with a direct negative influence on treatment success [8-11]. Hypoxia limits tumor cells' treatment response, rendering them radioresistant, and predisposes them towards metastases [12-13]. At present the methods available for assessing oxygen concentration directly in vivo are the Eppendorf electrode (Eppendorf AG, gold standard to assess tumor hypoxia) and the Oxylite probe (Oxford optronics) [11]. However, these techniques are invasive, technically demanding and operator-dependent [11, 14]. Therefore, they haven't gained wide acceptability in clinical practice. Another well-recognised factor of crucial significance in management and prognosis of NSCLC is the extent of the disease resulting in different patient staging. The most important determinants of disease stage and subsequently prognosis are the size of the tumor, lymph node infiltration and metastatic disease [2]. In particular, distant metastatic involvement automatically upgrades patients to stage IV rendering them candidates only for palliative treatment.

PET is a non-invasive modality that, after application of appropriate radiotracers, enables the evaluation of specific molecular processes like cellular metabolism, glycolytic rate, tumor hypoxia, perfusion or receptor expression in tumors. Fluorine-18 fluoromisonidazole (^{18}F-FMISO) is an extensively evaluated PET radiotracer in visualization of tumor hypoxia that has demonstrated a correlation between oxygen measurements and tracer uptake; ^{18}F-FMISO PET is nowadays considered a robust method in estimating the burden of hypoxia in the pO_2 range of a few mm Hg [3, 15-18]. Given the pivotal role of tumor hypoxia in cancer treatment response and prognosis, ^{18}F-FMISO PET seems to be a very promising modality in the evaluation of oncological patients. Nevertheless, despite its wide application, ^{18}F-FMISO remains a tracer, whose role in the diagnostic work-up of patients with NSCLC is still open. On the other hand, fluorine-18 fluorodeoxyglucose (^{18}F-FDG), the workhorse of PET imaging, is a biomarker of intracellular glucose metabolism, reflecting the tumor 'burden' of the malignancy. Numerous studies have highlighted the contribution of ^{18}F-FDG PET and PET/CT in the diagnostic approach, management and prognosis of lung cancer [19-22]. Dynamic PET/CT (dPET/CT) is a modality that allows registration of tracer kinetics over time and, after application of compartment modelling, enables the extraction of values of tracer kinetic parameters, which depict specific molecular processes [23]. Moreover, a non-compartment model can be applied leading to the estimation of fractal dimension (FD), a parameter reflecting heterogeneity [24]. This information is unattainable, when the classical whole body PET/CT protocols are performed, in which data are collected only at one time point after tracer injection.

It is known that in malignant cells glycolysis increases in hypoxia, especially in conditions of acute hypoxia. However, PET studies in several tumor types have shown that this relationship is not governed by a simple, linear pattern [25]. The purpose of this study was to evaluate and compare, by means of dynamic and static PET/CT, the distribution patterns and pharmacokinetics of ^{18}F-FDG, a biomarker of tumor glycolytic rate and viability, and of ^{18}F-FMISO, a biomarker of tumor hypoxia, in patients suffering from inoperable stage IIIB NSCLC. We aimed to detect potential statistically significant correlation between SUVs and kinetic parameters of the two radiopharmaceuticals that would reflect an indirect correlation between the mechanisms of glycolysis and hypoxia in NSCLC. Correlation analysis was also performed between parameters of each tracer. To our knowledge, no data have been published regarding the comparison between dynamic ^{18}F-FDG and ^{18}F-FMISO PET/CT studies.

Materials and methods

Patients

Thirteen patients (eleven male, two female) confirmed to suffer from inoperable stage III NSCLC were enrolled in the study. The histologic data of the patients was the following: four of them had adenocarcinoma while nine suffered from squamous cell carcinoma. Their mean age was 62.2 years (**Tables 1** and **2**). The included patients were not diabetic. None of them had

Table 1. Characteristics and main results derived from PET studies with ^{18}F-FDG of the patients investigated

Patient no.	Age (years)	Sex (M/F)	Histology	Metastases (Yes/No)	$SUV_{average}$	SUV_{max}	K_1	k_3	influx	FD
1	71	M	Adeno Ca	No	1.5	2.4	0.13	0.05	0.01	1.06
2	65	M	Adeno Ca	Yes	8.3	12.2	0.33	0.23	0.08	1.24
3	56	M	SCC	No	4.6	7.1	0.24	0.15	0.06	1.21
4	78	M	SCC	Yes	6.9	26.1	0.08	0.14	0.02	1.28
5	75	F	SCC	No	6.9	18.7	0.14	0.12	0.03	1.22
6	73	F	Adeno Ca	No	11.1	28.1	0.22	0.12	0.04	1.37
7	44	M	SCC	No	8.6	15.8	0.20	0.14	0.05	1.39
8	56	M	SCC	Yes	9.0	23.1	0.10	0.14	0.29	1.28
9	61	M	Adeno Ca	Yes	8.6	13.0	n.a.	n.a.	n.a.	n.a.
10	67	M	SCC	Yes	10.3	13.3	0.36	0.37	0.08	1.28
11	70	M	SCC	Yes	14.9	21.4	0.22	0.30	0.07	1.34
12	74	M	SCC	No	10.7	20.9	0.32	0.14	0.06	1.29
13	70	M	SCC	No	3.2	5.1	0.24	0.06	0.02	1.15

The quantitative values refer to mean ^{18}F-FDG values. Adeno Ca = adenocarcinoma; SCC = squamous cell carcinoma; n.a. = not acquired quantitative data (dynamic PET/CT study not performed due to patient discomfort).

Table 2. Characteristics and main results derived from PET studies with ^{18}F-FMISO of the patients investigated

Patient no.	Age (years)	Sex (M/F)	Histology	Metastases (Yes/No)	$SUV_{average}$	SUV_{max}	K_1	k_3	influx	FD
1	71	M	Adeno Ca	No	1.0	1.3	0.16	0.09	0.03	1.16
2	65	M	Adeno Ca	Yes	2.1	2.7	0.42	0.02	0.01	1.18
3	56	M	SCC	No	1.0	1.3	0.21	0.14	0.02	1.09
4	78	M	SCC	Yes	1.3	2.0	0.35	0.04	0.02	1.32
5	75	F	SCC	No	1.0	1.9	0.31	0.03	0.01	1.11
6	73	F	Adeno Ca	No	1.6	2.8	0.20	0.04	0.01	1.14
7	44	M	SCC	No	0.9	1.8	0.05	0.10	0.02	1.11
8	56	M	SCC	Yes	1.4	2.2	0.31	0.04	0.02	1.16
9	61	M	Adeno Ca	Yes	3.4	5.1	n.a.	n.a.	n.a.	n.a.
10	67	M	SCC	Yes	0.8	1.1	0.45	0.03	0.02	0.99
11	70	M	SCC	Yes	1.7	2.6	0.27	0.05	0.03	1.17
12	74	M	SCC	No	0.9	1.5	0.19	0.07	0.02	1.04
13	70	M	SCC	No	1.5	2.1	0.25	0.08	0.04	1.17

The quantitative values refer to mean ^{18}F-FMISO values. Adeno Ca = adenocarcinoma; SCC = squamous cell carcinoma; n.a. = not acquired quantitative data (dynamic PET/CT study not performed due to patient discomfort).

undergone chemotherapy. Patients gave written informed consent to participate in the study and to have their medical records released. The study was approved by the Ethical Committee of the University of Heidelberg and the Federal Agency for Radiation Protection (Bundesamt für Strahlenschutz).

Data acquisition

The double-tracer study in each patient was completed in two consecutive days. The patients were intravenously administered with a maximum of 250 MBq ^{18}F-FDG on the first day and respectively a maximum of 250 MBq ^{18}F-FMISO on the second day. Data acquisition consisted of two parts for each tracer: the dynamic part (dPET/CT studies) and the static part. dPET/CT studies were performed over the thorax for 60 minutes using a 28-frame protocol (10 frames of 30 seconds, 5 frames of 60 seconds, 5 frames of 120 seconds and 8 frames of 300 seconds). Additional static imag-

es from the maxilla to the proximal legs were acquired in the ^{18}F-FDG PET/CT studies and respectively from the maxilla to the pelvic entry in the ^{18}F-FMISO PET/CT studies. The image duration was 2 minutes per bed position for the emission scans. A dedicated PET/CT system (Biograph mCT, 128 S, Siemens Co., Erlangen, Germany) with an axial field of view of 21.6 cm with TruePoint and TrueV, operated in a three-dimensional mode, was used for patient studies. A low-dose attenuation CT (120 kV, 30 mA) was used for the attenuation correction of the dynamic emission PET data and for image fusion. A second low-dose CT (120 kV, 30 mA) was performed after the end of the dynamic series in order to avoid patient movement. The last images (55-60 minutes post-injection) were used for semi-quantitative analysis. All PET images were attenuation-corrected and an image matrix of 400 × 400 pixels was used for iterative image reconstruction. Iterative images reconstruction was based on the ordered subset expectation maximization algorithm (OSEM) with 2 iterations and 21 subsets as well as time of flight (TOF). The reconstructed images were converted to SUV images based on the formula [26]: SUV = tissue concentration (Bq/g)/(injected dose (Bq)/body weight (g)). The SUV 55 to 60 minutes postinjection served for quantification of the ^{18}F-FDG data.

Data analysis

Data analysis and evaluation consisted of visual analysis of the PET/CT scans, semi-quantitative evaluation based on SUV calculations, and quantitative analysis.

Qualitative analysis was based on visual assessment of the foci with enhanced tracer uptake on transaxial, coronal, and sagittal images for both PET/CT studies. The results of the two tracer PET/CTs were afterwards compared.

Semi-quantitative evaluation was based on volumes of interest (VOIs) and on the subsequent calculation of SUVs. VOIs were drawn with a 50% isocontour over foci of increased tracer uptake (primary tumor and potential metastatic lesions), reference tissue (normal lung parenchyma) and an arterial vessel (descending aorta). As previously mentioned, the global SUV was calculated according to the formula: SUV = tissue concentration (Bq/g)/(injected dose (Bq)/body weight (g)).

Quantitative evaluation of the dynamic PET/CT data was performed using a dedicated software [27, 28]. Time activity curves (TACs) were created using VOIs drawn with a 50% isocontour, placed over foci demonstrating pathological enhanced uptake. A two-tissue compartment model with a blood component (V_B) was used for the evaluation of the rate constants (K_1, k_2, k_3 and k_4) for both radiotracers [29, 30]. The two-tissue compartment model we applied is a modification of the one proposed by Sokoloff et al, which did not take into account the parameters k_4 and V_B [29]. This lack of k_4 and V_B however leads to different values of the parameters K_1 and k_3, since K_1 is dependent on V_B and k_3 on k_4. The model parameters were accepted when K_1, k_2, k_3 and k_4 were less than 1 and V_B exceeded zero. The unit for the rate constants K_1, k_2, k_3 and k_4 is 1/min, while V_B reflects the fraction of blood within the VOI. The global influx was also calculated, after applying the transport rates derived from the two-tissue compartment model analysis and using the formula: influx = $(K_1 \times k_3)/(k_2 + k_3)$. The input function was retrieved from the image data according to methods already reported in literature [31, 32]. One problem in patients is the accurate measurement of input function, which theoretically requires arterial blood sampling. It has been shown however, that input function can be accurately enough retrieved from image data [31]. For the input function, the mean value of the VOI data from the descending aorta was used. A vessel VOI consisted of at least seven ROIs in sequential PET/CT images. The recovery coefficient is 0.65 for a diameter of 10 mm and for the system described above using 2 iterations and 21 subsets [33]. Partial volume correction was not performed due to the very limited partial volume effects; this limitation is attributed to the high resolution, the small pixel size, the application of VOIs and the use of a large arterial vessel.

Furthermore, a non-compartment model was used in order to calculate the fractal dimension (FD). FD is a parameter for assessment of heterogeneity of the tracer kinetics and was calculated using the time activity data in each individual voxel of a VOI. The values of the FD vary from 0 to 2 showing the deterministic or chaotic distribution of the tracer activity via time in a local volume defined by a VOI. A subdivision of

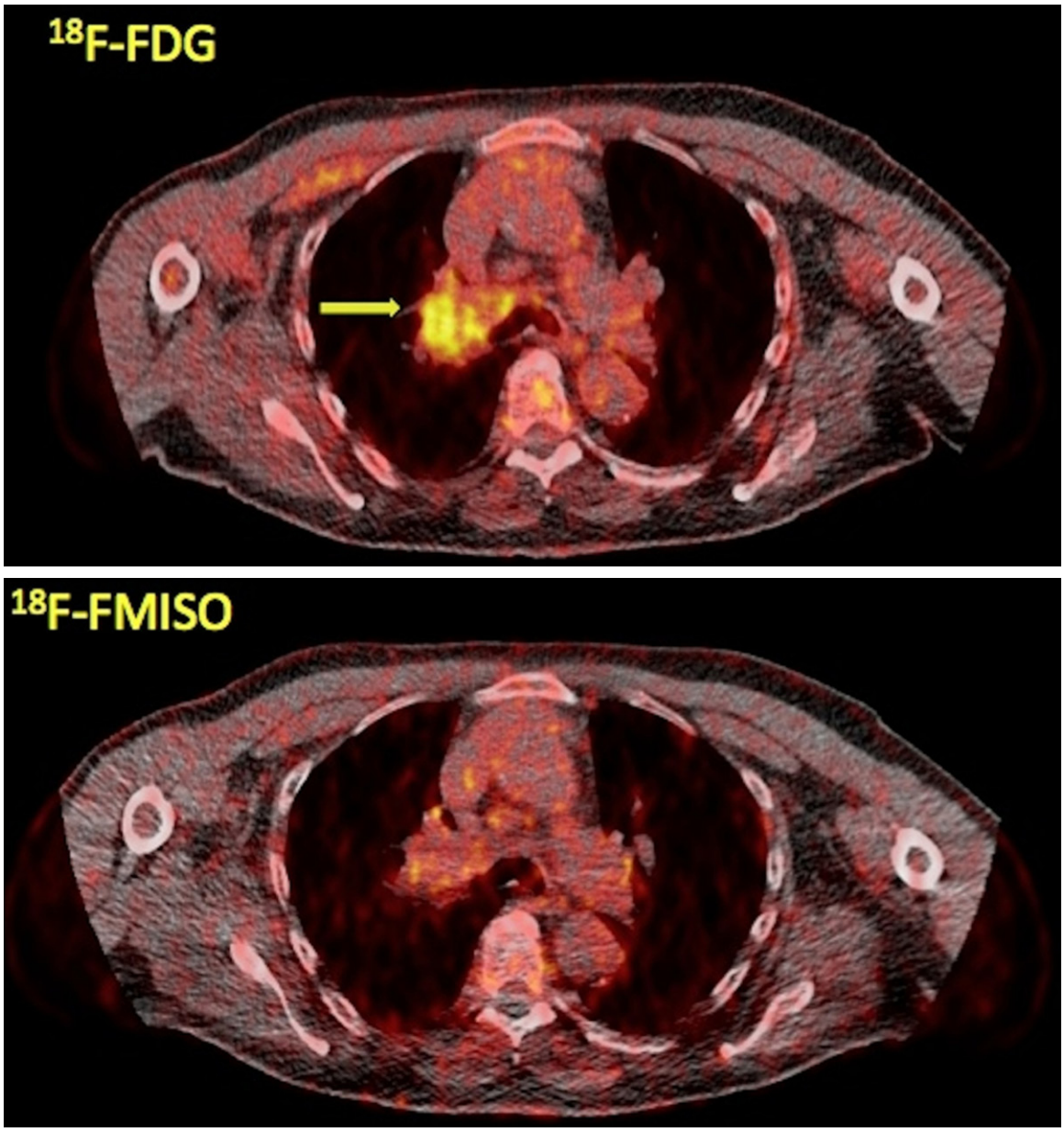

Figure 1. A 70-year-old male stage IIIB lung cancer patient referred to our department for PET/CT evaluation. Transaxial PET/CT images at the level of the lungs reveal the tumor in segment 3 of the right lung with enhanced ^{18}F-FDG uptake (upper row, arrow; $SUV_{average}$ = 3.2, SUV_{max} = 5.0) but with faint ^{18}F-FMISO accumulation (lower row; $SUV_{average}$ = 1.5, SUV_{max} = 2.1).

7 × 7 and a maximal SUV of 20 were applied for the calculation of FD [24].

Data were statistically evaluated using the STATA/SE 12.1 (StataCorp) software on an Intel Core (2· 3.06 GHz, 4 GB RAM) running with Mac OS X 10.8.4 (Apple Inc., Cupertino, CA, USA). The statistical evaluation was performed using descriptive statistics, box plots, Wilcoxon rank-sum test and Spearman's rank correlation analysis. The results were considered significant for p less than 0.05 ($p < 0.05$).

Results

Qualitative analysis

^{18}F-FDG PET/CT demonstrated enhanced tracer uptake in all thirteen primary lung tumors. The mean tumor diameter was 6.7 cm (range

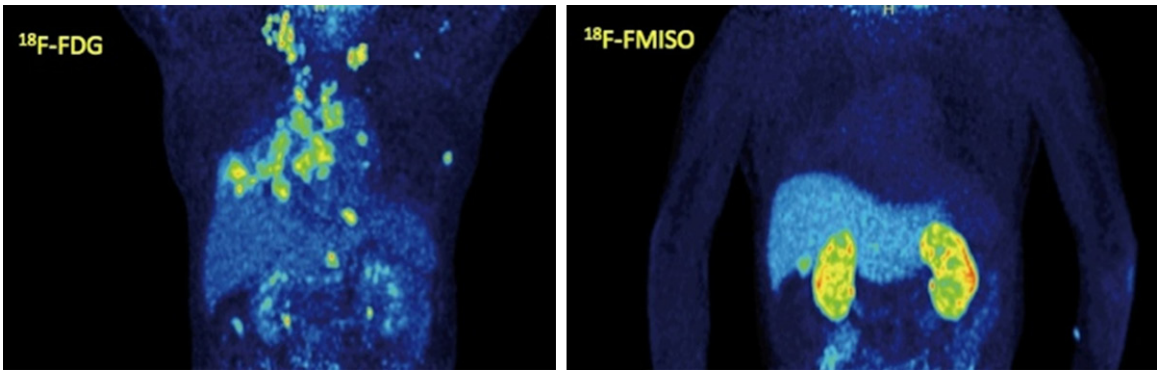

Figure 2. A 65-year-old patient suffering from stage IIIB NSCLC of the right lung (segment 5). Maximum intensity projection (MIP) images of ^{18}F-FDG PET/CT (left) and ^{18}F-FMISO PET/CT (right). ^{18}F-FDG PET/CT demonstrates the primary tumor as well as multiple hypermetabolic ^{18}F-FDG avid foci indicative of metastatic involvement of the supraclavicular lymph nodes, lymph nodes of the cervix, mediastinum and hilar region, as well as vertebrae of the thoracic spine and the scapula. On the other hand, ^{18}F-FMISO demonstrates the tumor with faint uptake and fails to reveal any metastases.

from 2.3 to 13 cm). In six patients it also revealed in total 43 metastatic lesions as sites of increased ^{18}F-FDG accumulation, leading to disease stage upgrading and subsequent alteration in patient management. On the other hand, ^{18}F-FMISO PET/CT depicted the 12/13 primary tumors with faint tracer uptake; only one tumor (adenocarcinoma) was ^{18}F-FMISO avid ($SUV_{average}$ = 3.4, SUV_{max} = 5.0). Moreover, ^{18}F-FMISO failed to show enhanced uptake in any of the 43 metastatic lesions that ^{18}F-FDG PET/CT revealed. **Figure 1** demonstrates an example of a patient with NSCLC of the right lung. ^{18}F-FDG PET/CT images showed enhanced ^{18}F-FDG uptake in the anatomical area of the primary tumor with a mean $SUV_{average}$ of 3.2. In the same patient ^{18}F-FMISO PET/CT revealed only faint ^{18}F-FMISO uptake in the tumor ($SUV_{average}$ = 1.5). **Figure 2** shows a patient with NSCLC of the segment 5 of the right lung. ^{18}F-FDG PET/CT revealed the primary tumor and metastatic involvement of the supraclavicular lymph nodes, lymph nodes of the cervix, mediastinum and hilar region, as well as of the osseous structures of the thorax (thoracic spine and scapula). On the other hand, ^{18}F-FMISO demonstrated the tumor with faint uptake and moreover it failed to depict the wide metastatic involvement. Treatment management was changed after the results of the ^{18}F-FDG PET/CT scan. **Figures 3** and **4** show a patient suffering from NSCLC of the left lung. The tumor is delineated by both ^{18}F-FDG and ^{18}F-FMISO, with respective mean SUVs of 8.6 and 3.4. Moreover, the patient demonstrated also metastases to contralateral mediastinal lymph nodes and the sternum, which were detected, however, only with ^{18}F-FDG PET/CT and not ^{18}F-FMISO PET/CT.

Quantitative analysis

The mean values of the primary tumors' kinetic parameters, derived after application of two-tissue compartment modelling on the ^{18}F-FDG dPET/CT data, were the following: $SUV_{average}$ = 8.9, SUV_{max} = 15.1, K_1 = 0.23 (1/min), k_2 = 0.53 (1/min), k_3 = 0.17 (1/min), k_4 = 0.02 (1/min), V_B = 0.09, influx = 0.05 (1/min). In comparison, the respective mean values of the lesions (only primary tumors) detected with ^{18}F-FMISO dPET/CT were: $SUV_{average}$ = 1.5, SUV_{max} = 2.2, K_1 = 0.26 (1/min), k_2 = 0.56 (1/min), k_3 = 0.06 (1/min), k_4 = 0.06 (1/min), V_B = 0.12, influx = 0.02 (1/min). **Tables 1-3** demonstrate analytically the results of the PET exams with both tracers. According to these results, $SUV_{average}$, SUV_{max}, k_3 and influx for ^{18}F-FDG were significantly higher than for ^{18}F-FMISO (**Table 4**). The results concerning the between tracers' differences were considered significant for p less than 0.05 ($p < 0.05$).

Fractal dimension (FD) was applied for further characterization of ^{18}F-FDG and ^{18}F-FMISO kinetics in primary tumors. The mean FD value was significantly higher for ^{18}F-FDG (FD = 1.25) than ^{18}F-FMISO (FD = 1.14), implying a higher degree of heterogeneity of tracer uptake.

As already mentioned, metastatic lesions were depicted in ^{18}F-FDG PET/CT but not in ^{18}F-FMISO

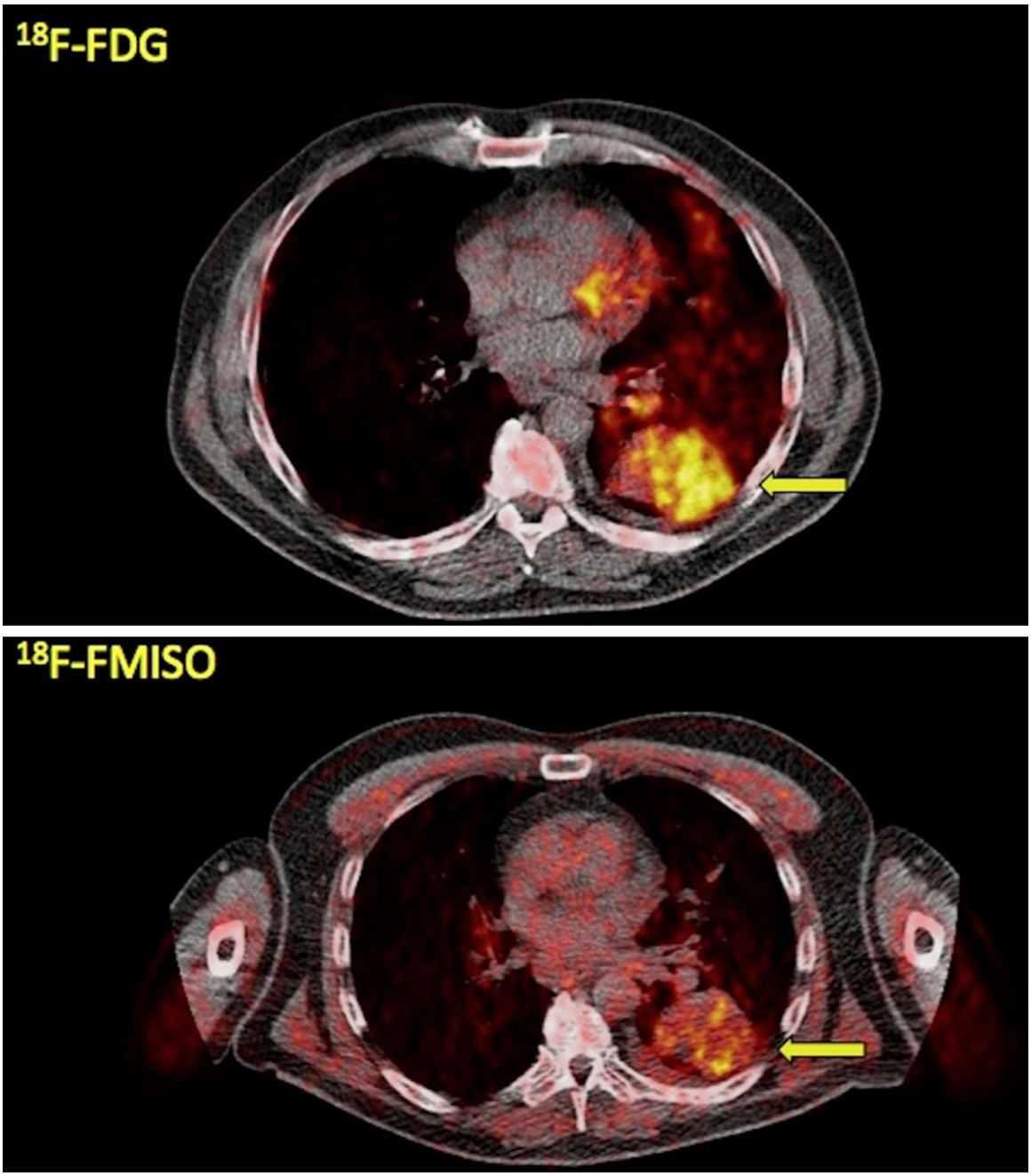

Figure 3. A 61-year-old patient with stage IIIB NSCLC of the left lung. Transaxial PET/CT images at the level of the lungs reveal the tumor in segment 6 of the left lung with enhanced tracer uptake both in ^{18}F-FDG PET/CT (arrow, upper row; $SUV_{average}$ = 8.6, SUV_{max} = 13.0) as well as in ^{18}F-FMISO PET/CT (arrow, lower row; $SUV_{average}$ = 3.4, SUV_{max} = 5.0).

PET/CT. The mean ^{18}F-FDG values of these lesions were the following: $SUV_{average}$ = 9.4, SUV_{max} = 14.6, K_1 = 0.25 (1/min), k_2 = 0.53 (1/min), k_3 = 0.19 (1/min), k_4 = 0.02 (1/min), V_B = 0.07, influx = 0.06 (1/min) and FD = 1.24.

We performed a Spearman's rank correlation analysis between ^{18}F-FDG and ^{18}F-FMISO kinetics: no significant correlation was observed between the two tracers' kinetic parameters (**Table 5**). Correlation analysis was also performed between SUVs and kinetic parameters for each tracer separately. In the case of ^{18}F-FDG the most significant correlations ($p < 0.05$) were found between FD and $SUV_{average}$ ($r = 0.86$), FD and SUV_{max} ($r = 0.70$), FD and influx ($r =$

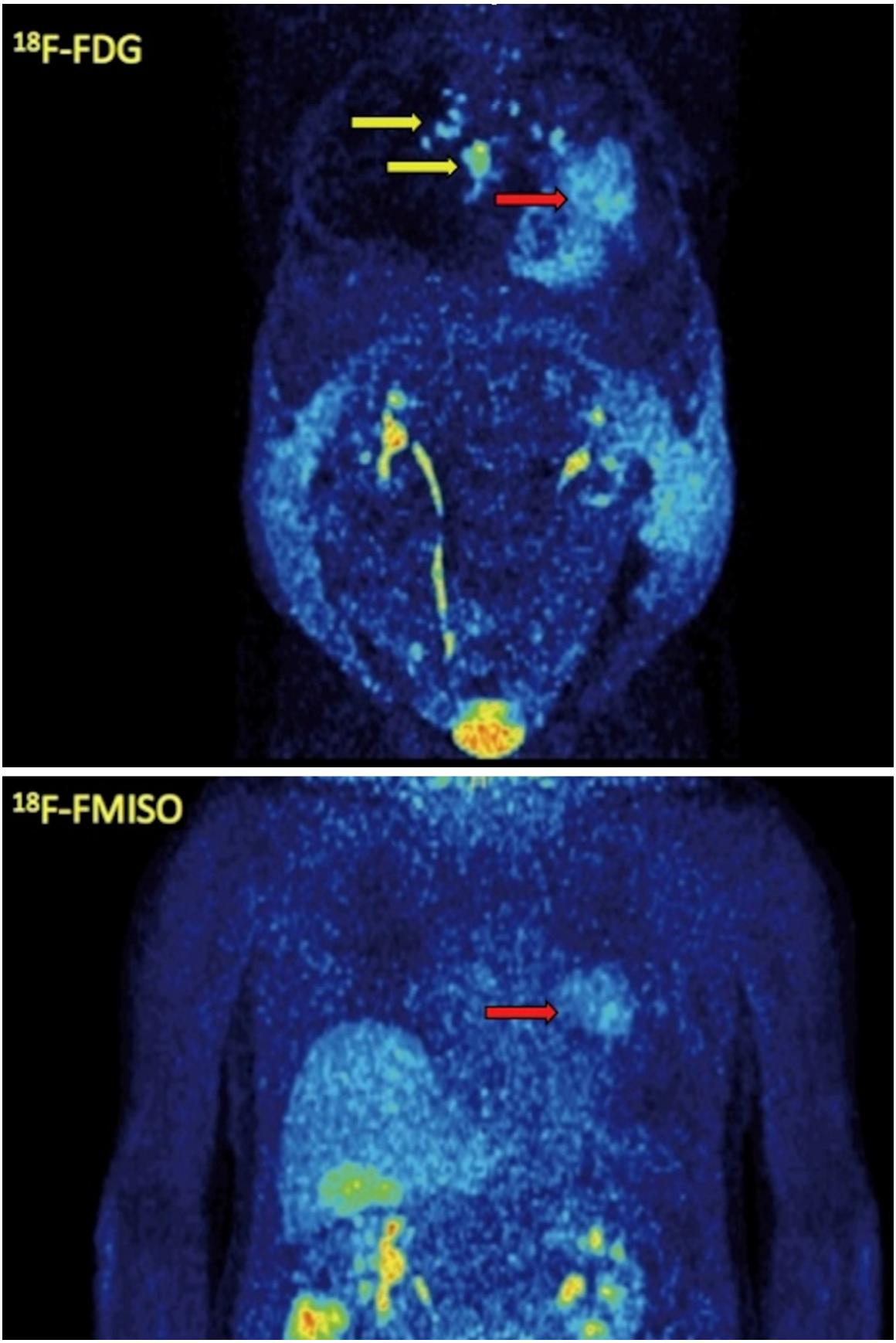
18F-FDG
18F-FMISO

Figure 4. MIP images of ^{18}F-FDG PET/CT (upper row) and ^{18}F-FMISO PET/CT (lower row) of the same patient as in **Figure 3.** The patient demonstrates, apart from the primary tumor (red arrow), metastases to contralateral mediastinal lymph nodes and the sternum (yellow arrows), which are depicted, however, only with ^{18}F-FDG PET/CT and not with ^{18}F-FMISO PET/CT. The patient developed also ascites due to the malignancy.

Table 3. Descriptive statistics of SUVs and kinetic parameters for ^{18}F-FDG and ^{18}F-FMISO in NSCLC patients. K_1, k_2, k_3, k_4 and influx expressed in (1/min). The values refer to primary tumors

Radiopharmaceutical	Parameters	Mean	Median	Minimum	Maximum
^{18}F-FDG	$SUV_{average}$	8.9	8.6	1.5	17.8
	SUV_{max}	15.1	14.6	2.4	28.1
	K_1	0.23	0.23	0.02	0.46
	k_2	0.53	0.59	0.37	0.67
	k_3	0.17	0.15	0.05	0.37
	k_4	0.02	0.01	0.00008	0.12
	V_B	0.09	0.05	0.0004	0.65
	influx	0.05	0.06	0.01	0.11
	FD	1.25	1.24	1.06	1.38
^{18}F-FMISO	$SUV_{average}$	1.5	1.3	0.8	3.4
	SUV_{max}	2.2	2.0	1.1	5.1
	K_1	0.26	0.26	0.05	0.45
	k_2	0.56	0.58	0.21	0.99
	k_3	0.06	0.05	0.02	0.14
	k_4	0.06	0.06	0.02	0.13
	V_B	0.12	0.09	0.002	0.59
	influx	0.02	0.02	0.01	0.04
	FD	1.14	1.15	0.99	1.32

0.40), influx and $SUV_{average}$ (r = 0.67), influx and K_1 (r = 0.58), influx and k_3 (r = 0.69), K_1 and SUV_{max} (r = -0.40), as well as between k_3 and $SUV_{average}$ (r = 0.57) (**Table 6**). In ^{18}F-FMISO the most significant correlations were observed between FD and $SUV_{average}$ (r = 0.78), FD and SUV_{max} (r = 0.63), influx and k_3 (r = 0.59), and between K_1 and k_3 (r = -0.76) (**Table 7**).

Discussion

Despite its low efficacy, radiation therapy combined with platinum-based chemotherapy is the standard treatment for inoperable NSCLC. This limited efficacy, however, can be ameliorated by intensifying radiation dose without causing significant toxicity [34]. Thus, the identification of factors that affect treatment outcome and predict therapy response is highly important. Tumor hypoxia is recognized as an independent factor of clinical outcome, which has been shown to increase resistance of malignant cells against radiation therapy, thus affecting the potency of the applied treatment [13, 14, 25]. The extent of the disease, in terms of lymph node infiltration and metastatic involvement, is also a factor of outmost significance in NSCLC patient management; the identification of previously unknown distant metastases automatically upgrades the patient to stage IV leading to radical changes in treatment and prognosis. It is therefore crucial to carefully evaluate and subsequently select those unresectable NSCLC patients, who are candidates for radiotherapy and are expected to benefit most from this treatment. In the present study, we examined a series of patients suffering from unresectable stage IIIB NSCLC scheduled for intensity modulated radiation therapy (IMRT) by means of dynamic and static PET/CT, in order to acquire information regarding tumor burden (by means of glycolytic rate), hypoxia and potential metastatic involvement. For this reason we applied two different PET radiotracers proven to reflect sufficiently these mechanisms; ^{18}F-FDG, a glucose analogue, which serves as a biomarker of tumor viability and aggressiveness and ^{18}F-FMISO, a thoroughly investigated tracer for visualization of tumor hypoxia.

Our results demonstrated the high efficacy of ^{18}F-FDG PET/CT in detecting malignant disease and its actual extent; six subjects had in total 43 previously unknown, related to the primary tumor, metastases and were therefore excluded from planned IMRT. These results are in accordance with reported data regarding the potency of ^{18}F-FDG PET and PET/CT in NSCLC and the pivotal role of the technique in the diagnostic work-up of this malignancy. ^{18}F-FDG PET is a standard modality for staging NSCLC and results in a different disease stage than the one determined by standard methods in over

Table 4. Results of the Wilcoxon rank-sum test for the probability of differences between ^{18}F-FDG and ^{18}F-FMISO

		^{18}F-FMISO parameters					
		$SUV_{average}$	SUV_{max}	K_1	k_3	influx	FD
^{18}F-FDG parameters	$SUV_{average}$	p < 0.0001*					
	SUV_{max}		p < 0.0001*				
	K_1			p = 0.218			
	k_3				p = 0.001*		
	influx					p = 0.027*	
	FD						p = 0.007*

*Significant probabilities (p < 0.05).

half patients, leading to alterations in patient management [35]. Particularly in regard with M-staging, ^{18}F-FDG PET demonstrates a sensitivity of 94% and a specificity of 97% [20].

On the other hand, ^{18}F-FMISO, despite being the most widely used nitroimidazole imaging agent, is a tracer without a clear role yet in the diagnostic algorithm of NSCLC. ^{18}F-FMISO PET/CT provides information on tumor hypoxia and thus, as an index of tissue oxygenation, can potentially aid in radiotherapy planning and disease prognosis, given the leading role of hypoxia in radiation resistance. FMISO enters the cells by passive diffusion, with its lipophilicity being a major determinant of the intracellular penetration. The tracer is intracellularly reduced by nitroreductase enzymes and becomes then trapped in cells with reduced oxygen partial pressure, resulting in tracer accumulation. On the other hand, in normally oxygenated cells, the parent compound is regenerated by reoxidation and no metabolite accumulation takes place [36, 37]. The results of our study revealed a high ^{18}F-FMISO retention (by visual evaluation) in only 1/13 primary tumors and in none of the 43 metastases (mean $SUV_{average}$ = 1.5, mean SUV_{max} = 2.2). It is very likely, that this small tracer accumulation in the tumor area may be due to the scanning protocol followed (lack of late imaging). The lack of late imaging is the major limitation of the study (see below), since ^{18}F-FMISO carries the inherent disadvantages of slow accumulation in the hypoxic lesions and limited normal tissue clearance, which limit its clinical use [38]. However, the mean and median ^{18}F-FMISO SUV are in accordance with respective values derived from previous ^{18}F-FMISO PET studies despite the lack of acquisition of images at 2 hours post injection (p.i.) or later. Eschmann et al. reported that in 14 NSCLC patients the mean $SUV_{average}$ was 1.62 at 2 hours and 1.80 at 4 hours p.i.. The respective values for SUV_{max} were 2.09 and 2.40 [14]. In a prospective study by Cherk et al. 21 patients with suspected or biopsy-proven NSCLC underwent ^{18}F-FDG and ^{18}F-FMISO PET. Their results demonstrated that ^{18}F-FMISO tumor uptake was significantly less the ^{18}F-FDG uptake, while the mean ^{18}F-FMISO SUV_{max} at 2 hours p.i. was 1.20. Moreover, no correlation was found between the two tracers' SUV_{max} [39]. Further, our semi-quantitative results are similar with those derived from head and neck cancer patients, in which the highest so far experience has been gained, regarding hypoxia imaging. Thorwarth et al. performed dynamic ^{18}F-FMISO PET scans in 15 patients and resulted in a median SUV_{max} of 2.25 at 4 hours p.i. [40]. Hicks et al reported a mean ^{18}F-FMISO SUV_{max} of 2.5 ± 0.5 at 2 hours p.i. (range from 1.6 to 3.5) in 15 head and neck cancer patients. The authors applied a SUV_{max} of 1.6 as a threshold for characterizing a primary tumor as hypoxic [41]. Tachibana et al. studied a group of ten cancer patients (four with head and neck cancer, four with gastrointestinal cancers, one with lung cancer and one with uterine cancer) and concluded that mean tumor SUV_{max} was similar for 100 min and 180 minutes p.i. (2.33 ± 0.72 and 2.28 ± 0.61 respectively) [42].

A two-tissue compartment model was applied for evaluation of the kinetics of both tracers. The application of this model leads to the extraction of the kinetic parameters K_1, k_2, k_3, k_4, influx (K_i) and fractional blood volume (V_B), also called vessel density. In the case of ^{18}F-FDG K_1 reflects the influx while k_2 reflects the efflux of the tracer, and k_3 represents its phosphorylation rate while k_4 its dephosphorylation rate. Influx (K_i) is derived from the equation = $(K_1 \times k_3)/(k_2 + k_3)$. The application of the two-

Table 5. Results of the Spearman's rank correlation analysis between quantitative and semi-quantitative (SUVs) parameters of ^{18}F-FDG and ^{18}F-FMISO. Values were considered significant for $p < 0.05$. No statistically significant correlation between the two tracers' parameters is demonstrated

		^{18}F-FMISO parameters					
		$SUV_{average}$	SUV_{max}	K_1	k_3	influx	FD
^{18}F-FDG parameters	$SUV_{average}$	0.201 (p = 0.555)	0.556 (p = 0.082)	-0.009 (p = 0.979)	-0.373 (p = 0.259)	-0.373 (p = 0.259)	-0.227 (p = 0.502)
	SUV_{max}	0.173 (p = 0.611)	0.547 (p = 0.082)	0.264 (p = 0.433)	-0.509 (p = 0.110)	-0.310 (p = 0.235)	0.036 (p = 0.916)
	K_1	0.173 (p = 0.611)	0.082 (p = 0.811)	-0.055 (p = 0.873)	0.055 (p = 0.873)	-0.082 (p = 0.811)	-0.227 (p = 0.502)
	k_3	0.292 (p = 0.384)	0.228 (p = 0.501)	0.364 (p = 0.272)	-0.118 (p = 0.729)	-0.127 (p = 0.709)	0.027 (p = 0.937)
	influx	0.228 (p = 0.501)	0.246 (p = 0.466)	0.109 (p = 0.750)	-0.118 (p = 0.729)	-0.346 (p = 0.298)	-0.264 (p = 0.433)
	FD	-0.009 (p = 0.979)	0.392 (p = 0.233)	-0.182 (p = 0.593)	-0.146 (p = 0.670)	-0.427 (p = 0.190)	-0.209 (p = 0.537)

Table 6. Results of the Spearman's rank correlation analysis between quantitative and semi-quantitative (SUVs) parameters of ^{18}F-FDG. Values were considered significant for $p < 0.05$

	$SUV_{average}$	SUV_{max}	K_1	k_3	V_B	influx	FD
$SUV_{average}$							
SUV_{max}	0.6337*						
K_1	0.1484	-0.3974*					
k_3	0.5739*	0.3034	0.0580				
V_B	-0.0073	-0.2570	0.0647	0.0855			
influx	0.6697*	0.0421	0.5781*	0.6905*	0.2473		
FD	0.8596*	0.7021*	-0.0220	0.3785	0.0263	0.3968*	

*Significant correlation ($p < 0.05$).

Table 7. Results of the Spearman's rank correlation analysis between quantitative and semi-quantitative (SUVs) parameters of ^{18}F-FMISO. Values were considered significant for $p < 0.05$

	$SUV_{average}$	SUV_{max}	K_1	k_3	V_B	influx	FD
$SUV_{average}$							
SUV_{max}	0.8667*						
K_1	0.1786	0.1576					
k_3	-0.2382	-0.4343	-0.7552*				
V_B	-0.2032	-0.1611	-0.0559	0.2378		-	
influx	0.0490	-0.3082	-0.1678	0.5874*	0.1678		
FD	0.7811*	0.6270*	0.2448	-0.1608	-0.1826	0.1259	

*Significant correlation ($p < 0.05$).

tissue compartment model in ^{18}F-FMISO leads also to the extraction of kinetic parameters, which however reflect different molecular mechanisms than ^{18}F-FDG. In the case of ^{18}F-FMISO, indices K_1 and k_2 describe the influx and efflux of the radiopharmaceutical into out of the cells, while k_3 and k_4 represent the trapping and re-oxygenation of ^{18}F-FMISO [3]. Our results showed that $SUV_{average}$, SUV_{max}, k_3 and influx were significantly higher in ^{18}F-FDG than in ^{18}F-FMISO. Moreover, correlation analysis performed between the tracers' kinetic parameters demonstrated no significant correlation. This result is of no surprise, since ^{18}F-FMISO is a much more specific agent in comparison to the non-specific nature of ^{18}F-FDG [18]. As already mentioned, hypoxia is a general factor affecting glucose metabolism and moreover ^{18}F-FDG has been proposed to be a surrogate marker of tumor hypoxia [43]. However, it has been shown that tumor cell response to the phenomenon of hypoxia leads to differences between hypoxia (depicted with ^{18}F-FMISO) and glycolytic rate (depicted with ^{18}F-FDG), resulting in discordance in tracer uptake [18, 25]. Our results are in accordance with these previous findings, since, on one side, they reflect an intense glycolytic rate in the vast majority of the studied tumors and on the other side, they demonstrate no significant correlation between the tracers' kinetic parameters and SUVs.

Apart from applying a two-tissue compartment model for evaluation of tracers' kinetics, we also performed a non-compartmental approach leading to the extraction of fractal dimension (FD), an index representative of tissue heterogeneity. This parameter is based on the box counting procedure of the chaos theory for the analysis of dPET data [24]. The basic concept of this approach is that an increased FD is indicative of a more chaotic tracer distribution, correlating to higher tissue heterogeneity. In the present study, the FD values in lesions showed a statistically significant difference, with a mean FD value of 1.25 for ^{18}F-FDG and of 1.14 for ^{18}F-FMISO. Furthermore, as already mentioned, both in ^{18}F-FDG and ^{18}F-FMISO, FD demonstrated a highly significant correlation with various tracer parameters: in ^{18}F-FDG with $SUV_{average}$ ($r = 0.86$), SUV_{max} ($r = 0.70$) and influx ($r = 0.40$) and in ^{18}F-FMISO with $SUV_{average}$ ($r = 0.78$) and SUV_{max} ($r = 0.63$). This high correlation between FD and SUVs is in agreement with previous results from our group, regarding ^{18}F-FDG and ^{18}F-NaF PET/CT studies in multiple myeloma; in this, also double-tracer, study FD from myelomatous lesions demonstrated a highly significant correlation with $SUV_{average}$ both in ^{18}F-FDG ($r = 0.93$) as well as in ^{18}F-NaF ($r = 0.97$) PET/CT exams [44]. It is our belief that the application of this non-compartment derived parameter can aid in evaluation of complicated oncological differential diagnosis issues.

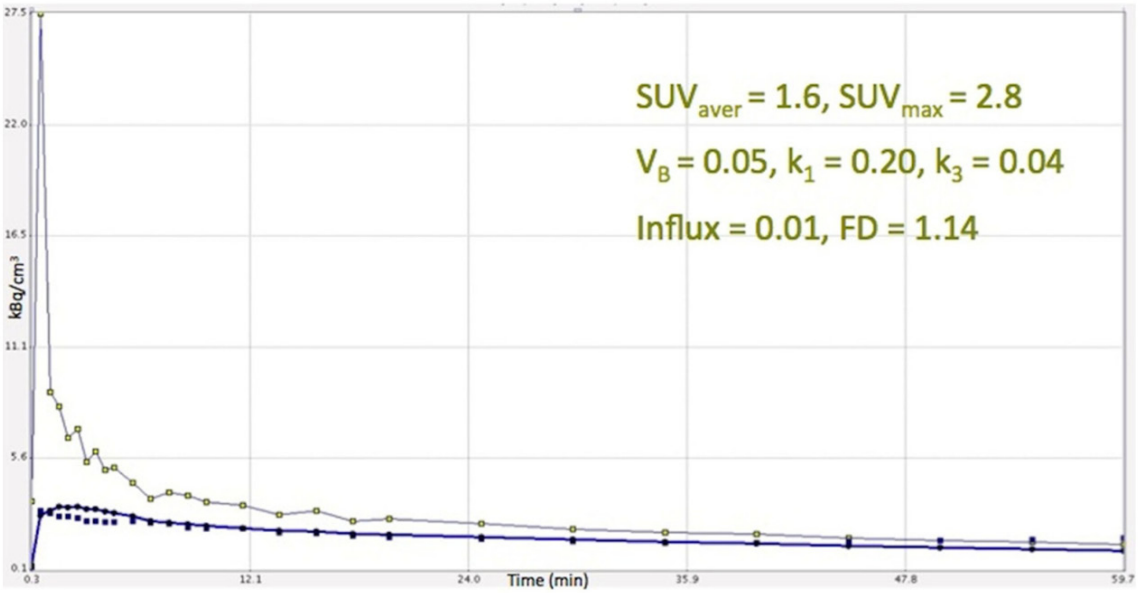

Figure 5. Time activity curve of ^{18}F-FMISO derived from a primary lung tumor, after application of two-tissue compartment modelling in the respective VOIs. The tracer's increase over time in the lesion is low and remains so during the whole acquisition time (60 min).

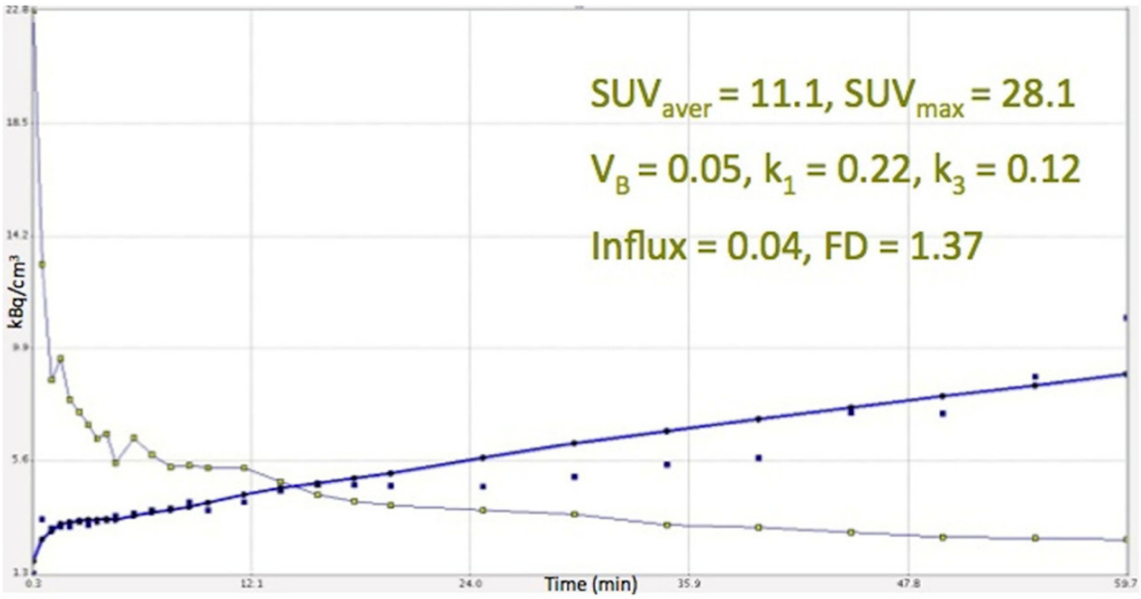

Figure 6. Time activity curve of ^{18}F-FDG derived from the same lung tumor as in **Figure 5**, after application of two-tissue compartment modelling in the respective VOIs. The tracer's increase is significantly higher than the respective rhythm of ^{18}F-FMISO.

Limitations

As already mentioned, the major limitation of our study is the lack, due to practical reasons, of delayed imaging (e.g. 2 h and 4 hour p.i.) concerning the ^{18}F-FMISO PET/CT imaging. Our studies involved dynamic acquisition for 60 minutes and then whole-body static imaging. This limitation may be important in ^{18}F-FMISO, due to the slow kinetics of tracer retention resulting in high background activity over the first 60 minutes. However, due to the low FMISO

uptake in the normal surrounding lung parenchyma, the uptake in the tumor was clearly visible, but low. Nevertheless, we tried to overcome this obstacle with the employment of time-activity curves (TACs) derived from VOIs placed over the lung tumors after application of two-tissue compartment modelling. With the exception of one tumor that showed intense ^{18}F-FMISO accumulation, the TACs derived from all other primary tumors demonstrated a steady low increase in which the tracer is concentrated over time in the lesion (**Figure 5**). Based on the behaviour of the tracer during the first 60 minutes, we assume that this steady low increase of ^{18}F-FMISO accumulation in the tumor area would not change significantly if late acquisition would be performed. This is in accordance to other studies mentioned before [14, 39-42]. In contrary to the TACs derived from ^{18}F-FMISO, the respective TACs from ^{18}F-FDG showed a steady increase reflecting the increase of tracer accumulation during dynamic PET acquisition (**Figure 6**). Another limitation was the small number of patients included.

Conclusion

We performed a double-tracer PET/CT study with the agents ^{18}F-FDG and ^{18}F-FMISO in patients with advanced NSCLC scheduled for IMRT. In terms of clinical practice, our results confirmed the utility of ^{18}F-FDG PET/CT in the diagnostic approach of the malignancy by excluding 6/13 (46%) patients with distant metastases from radical radiation treatment. On the other hand, imaging with ^{18}F-FMISO PET/CT didn't significantly aid in the management of our patient group. Only one subject demonstrated increased ^{18}F-FMISO tumor uptake, reflecting its potential sensitivity to radiotherapy. Based on the pharmacokinetic results, the lack of correlation between ^{18}F-FDG and ^{18}F-FMISO implies the discordance between increased glycolysis and hypoxia in the malignancy. To our knowledge this is the first study evaluating the distribution patterns and pharmacokinetics of these two tracers in NSCLC by means of dynamic PET/CT scanning. It is an undisputable fact that further studies are warranted in order to clarify the potential role of ^{18}F-FMISO PET/CT in the diagnostic workup and management of the malignancy as already proposed [14, 45, 46].

Disclosure of conflict of interest

The authors declare that they have no conflict of interest.

Address correspondence to: Dr. Christos Sachpekidis, Medical PET Group - Biological Imaging, Clinical Cooperation Unit Nuclear Medicine, German Cancer Research Center, Im Neuenheimer Feld 280, D-69210 Heidelberg. E-mail: christos_saxpe@yahoo.gr; c.sachpekidis@dkfz.de

References

[1] American Cancer Society: Cancer Facts and Figures 2014. Atlanta, Ga: American Cancer Society, 2014.

[2] Sequist LV. Non-small cell lung cancer. In: Chabner BA, Lynch TJ Jr, Longo DL, editors. Harrison's Manual of Oncology. McGraw-Hill Companies, Inc.; 2008. pp. 455-468.

[3] Askoxylakis V, Dinkel J, Eichinger M, Stieltjes B, Sommer G, Strauss LG, Dimitrakopoulou-Strauss A, Kopp-Schneider A, Haberkorn U, Huber PE, Bischof M, Debus J and Thieke C. Multimodal hypoxia imaging and intensity modulated radiation therapy for unresectable non-small-cell lung cancer: the HIL trial. Radiat Oncol 2012; 7: 157.

[4] Chemotherapy in non-small cell lung cancer: a meta-analysis using updated data on individual patients from 52 randomised clinical trials. Non-small Cell Lung Cancer Collaborative Group. BMJ 1995; 311: 899-909.

[5] Rowell NP and O'rourke NP. Concurrent chemoradiotherapy in non-small cell lung cancer. Cochrane Database Syst Rev 2004; 4: CD002140.

[6] Anderson CS and Curran WJ. Combined modality therapy for stage III non-small-cell lung cancer. Semin Radiat Oncol 2010; 20: 186-191.

[7] National Cancer Institute. Available at: Accessed March 22 2014.

[8] Brizel DM, Scully SP, Harrelson JM, Layfield LJ, Bean JM, Prosnitz LR and Dewhirst MW. Tumor oxygenation predicts for the likelihood of distant metastases in human soft tissue sarcoma. Cancer Res 1996; 56: 941-943.

[9] Movsas B, Chapman JD, Hanlon AL, Horwitz EM, Greenberg RE, Stobbe C, Hanks GE and Pollack A. Hypoxic prostate/muscle pO2 ratio predicts for biochemical failure in patients with prostate cancer: preliminary findings. Urology 2002; 60: 634-639.

[10] Brizel DM, Sibley GS, Prosnitz LR, Scher RL and Dewhirst MW. Tumor hypoxia adversely affects the prognosis of carcinoma of the head and neck. Int J Radiat Oncol Biol Phys 1997; 38: 285-289.

[11] Wang W, Lee NY, Georgi JC, Narayanan M, Guillem J, Schöder H and Humm JL. Pharmacokinetic analysis of hypoxia (18)F-fluoromisonidazole dynamic PET in head and neck cancer. J Nucl Med 2010; 51: 37-45.
[12] Graves EE, Maity A and Le QT. The tumor microenvironment in non-small-cell lung cancer. Semin Radiat Oncol 2010; 20: 156-163.
[13] Vaupel P and Mayer A. Hypoxia in cancer: significance and impact on clinical outcome. Cancer Metastasis Rev 2007; 26: 225-239.
[14] Eschmann SM, Paulsen F, Reimold M, Dittmann H, Welz S, Reischl G, Machulla HJ and Bares R. Prognostic impact of hypoxia imaging with 18F-misonidazole PET in non-small cell lung cancer and head and neck cancer before radiotherapy. J Nucl Med 2005; 46: 253-260.
[15] Chapman JD, Baer K and Lee J. Characteristics of the metabolism-induced binding of misonidazole to hypoxic mammalian cells. Cancer Res 1983; 43: 1523-1528.
[16] Koh WJ, Rasey JS, Evans ML, Grierson JR, Lewellen TK, Graham MM, Krohn KA and Griffin TW. Imaging of hypoxia in human tumors with [F-18]fluoromisonidazole. Int J Radiat Oncol Biol Phys 1992; 22: 199-212.
[17] Rasey JS, Koh WJ, Grierson JR, Grunbaum Z and Krohn KA. Radiolabelled fluoromisonidazole as an imaging agent for tumor hypoxia. Int J Radiat Oncol Biol Phys 1989; 17: 985-991.
[18] Rajendran JG, Schwartz DL, O'Sullivan J, Peterson LM, Ng P, Scharnhorst J, Grierson JR and Krohn KA. Tumor hypoxia imaging with [F-18] fluoromisonidazole positron emission tomography in head and neck cancer. Clin Cancer Res 2006; 12: 5435-5441.
[19] Gould MK, Maclean CC, Kuschner WG, Rydzak CE and Owens DK. Accuracy of positron emission tomography for diagnosis of pulmonary nodules and mass lesions: a meta-analysis. JAMA 2001; 285: 914-924.
[20] van Tinteren H, Hoekstra OS, Smit EF, van den Bergh JH, Schreurs AJ, Stallaert RA, van Velthoven PC, Comans EF, Diepenhorst FW, Verboom P, van Mourik JC, Postmus PE, Boers M and Teule GJ. Effectiveness of positron emission tomography in the preoperative assessment of patients with suspected non-small-cell lung cancer: the PLUS multicentre randomised trial. Lancet 2002; 359: 1388-1393.
[21] Lardinois D, Weder W, Hany TF, Kamel EM, Korom S, Seifert B, von Schulthess GK and Steinert HC. Staging of non-small-cell lung cancer with integrated positron-emission tomography and computed tomography. N Engl J Med 2003; 348: 2500-2507.
[22] Vansteenkiste J, Fischer BM, Dooms C and Mortensen J. Positron-emission tomography in prognostic and therapeutic assessment of lung cancer: systematic review. Lancet Oncol 2004; 5: 531-540.
[23] Dimitrakopoulou-Strauss A, Pan L and Strauss LG. Quantitative approaches of dynamic FDG-PET and PET/CT studies (dPET/CT) for the evaluation of oncological patients. Cancer Imaging 2012; 12: 283-289.
[24] Dimitrakopoulou-Strauss A, Strauss LG, Mikolajczyk K, Burger C, Lehnert T, Bernd L and Ewerbeck V. On the fractal nature of dynamic positron emission tomography (PET) studies. World J Nucl Med 2003; 2: 306-313.
[25] Rajendran JG, Mankoff DA, O'Sullivan F, Peterson LM, Schwartz DL, Conrad EU, Spence AM, Muzi M, Farwell DG and Krohn KA. Hypoxia and glucose metabolism in malignant tumors: evaluation by [18F]fluoromisonidazole and [18F] fluorodeoxyglucose positron emission tomography imaging. Clin Cancer Res 2004; 10: 2245-2252.
[26] Strauss LG and Conti PS. The applications of PET in clinical oncology. J Nucl Med 1991; 32: 623-648.
[27] Burger C and Buck A. Requirements and implementations of a flexible kinetic modeling tool. J Nucl Med 1997; 38: 1818-1823.
[28] Mikolajczyk K, Szabatin M, Rudnicki P, Grodzki M and Burger C. A Java environment for medical image data analysis: initial application for brain PET quantitation. Med Inform1998; 23: 207-214.
[29] Sokoloff L and Smith CB. Basic principles underlying radioisotopic methods for assay of biochemical processes in vivo. In: Greitz T, Ingvar DH, Widén L, editors. The metabolism of the human brain studied with positron emission tomography. New York: Raven Press; 1983; pp. 123-148.
[30] Miyazawa H, Osmont A, Petit-Taboué MC, Tillet I, Travère JM, Young AR, Barré L, MacKenzie ET and Baron JC. Determination of 18F-fluoro-2-deoxy-D-glucose rate constants in the anesthetized baboon brain with dynamic positron tomography. J Neurosci Methods 1993; 50: 263-272.
[31] Ohtake T, Kosaka N, Watanabe T, Yokoyama I, Moritan T, Masuo M Iizuka M, Kozeni K, Momose T and Oku S. Noninvasive method to obtain input function for measuring tissue glucose utilization of thoracic and abdominal organs. J Nucl Med 1991; 32: 1432-1438.
[32] Strauss LG, Klippel S, Pan L, Schönleben K, Haberkorn U and Dimitrakopoulou-Strauss A. Assessment of quantitative FDG PET data in primary colorectal tumours: which parameters are important with respect to tumour detection? Eur J Nucl Med Mol Imaging 2007; 34: 868-877.

[33] Jakoby BW, Bercier Y, Conti M, Casey ME, Bendriem B and Townsend DW. Physical and clinical performance of the mCT time-of-flight PET/CT scanner. Phys Med Biol 2011; 56: 2375-2389.

[34] Bradley JD, Moughan J, Graham MV, Byhardt R, Govindan R, Fowler J, Purdy JA, Michalski JM, Gore E and Choy H. A phase I/II radiation dose escalation study with concurrent chemotherapy for patients with inoperable stages I to III non-small-cell lung cancer: phase I results of RTOG 0117. Int J Radiat Oncol Biol Phys 2010; 77: 367-372.

[35] Pieterman RM, van Putten JW, Meuzelaar JJ, Mooyaart EL, Vaalburg W, Koëter GH, Fidler V, Pruim J and Groen HJ. Preoperative staging of non-small-cell lung cancer with positron-emission tomography. N Engl J Med 2000; 343: 254-261.

[36] Nunn A, Linder K and Strauss HW. Nitroimidazoles and imaging hypoxia. Eur J Nucl Med 1995; 22: 265-280.

[37] Lee ST and Scott AM. Hypoxia positron emission tomography imaging with 18f-fluoromisonidazole. Semin Nucl Med 2007; 37: 451-461.

[38] van Elmpt W, Zegers CM, Das M and De Ruysscher D. Imaging techniques for tumour delineation and heterogeneity quantification of lung cancer: overview of current possibilities. J Thorac Dis 2014; 6: 319-327.

[39] Cherk MH, Foo SS, Poon AM, Knight SR, Murone C, Papenfuss AT, Sachinidis JI, Saunder TH, O'Keefe GJ and Scott AM. Lack of correlation of hypoxic cell fraction and angiogenesis with glucose metabolic rate in non-small cell lung cancer assessed by 18F-Fluoromisonidazole and 18F-FDG PET. J Nucl Med 2006; 47: 1921-1926.

[40] Thorwarth D, Eschmann SM, Scheiderbauer J, Paulsen F and Alber M. Kinetic analysis of dynamic 18F-fluoromisonidazole PET correlates with radiation treatment outcome in head-and-neck cancer. BMC Cancer 2005; 5: 152.

[41] Hicks RJ, Rischin D, Fisher R, Binns D, Scott AM and Peters LJ. Utility of FMISO PET in advanced head and neck cancer treated with chemoradiation incorporating a hypoxia-targeting chemotherapy agent. Eur J Nucl Med Mol Imaging 2005; 32: 1384-1391.

[42] Tachibana I, Nishimura Y, Shibata T, Kanamori S, Nakamatsu K, Koike R, Nishikawa T, Ishikawa K, Tamura M and Hosono M. A prospective clinical trial of tumor hypoxia imaging with 18F-fluoromisonidazole positron emission tomography and computed tomography (F-MISO PET/CT) before and during radiation therapy. J Radiat Res 2013; 54: 1078-1084.

[43] Minn H, Clavo AC and Wahl RL. Influence of hypoxia on tracer accumulation in squamous-cell carcinoma: in vitro evaluation for PET imaging. Nucl Med Biol 1996; 23: 941-946.

[44] Sachpekidis C, Goldschmidt H, Hose D, Pan L, Cheng C, Kopka K, Haberkorn U and Dimitrakopoulou-Strauss A. PET/CT studies of multiple myeloma using ^{18}F-FDG and ^{18}F-NaF: comparison of distribution patterns and tracers' pharmacokinetics. Eur J Nucl Med Mol Imaging 2014; 41: 1343-1353.

[45] Bollineni VR, Wiegman EM, Pruim J, Groen HJ and Langendijk JA. Hypoxia imaging using Positron Emission Tomography in non-small cell lung cancer: implications for radiotherapy. Cancer Treat Rev 2012; 38: 1027-1032.

[46] Gagel B, Reinartz P, Demirel C, Kaiser HJ, Zimny M, Piroth M, Pinkawa M, Stanzel S, Asadpour B, Hamacher K, Coenen HH, Buell U and Eble MJ. [18F] fluoromisonidazole and [18F] fluorodeoxyglucose positron emission tomography in response evaluation after chemo-/radiotherapy of non-small-cell lung cancer: a feasibility study. BMC Cancer 2006; 6: 51.